Strong longitudinal color-field effects in pp collisions at energies available at the CERN Large Hadron Collider

V. Topor Pop, M. Gyulassy, J. Barrette, C. Gale, and A. Warburton

Phys. Rev. C **83**, 024902 — Published 7 February 2011

DOI: 10.1103/PhysRevC.83.024902

Strong longitudinal color-field effects in pp collisions at energies available at the CERN Large Hadron Collider.

V. Topor Pop,[1] M. Gyulassy,[2] J. Barrette,[1] C. Gale,[1] and A. Warburton[1]

[1]*McGill University, Montreal, Canada, H3A 2T8*

[2]*Columbia University, New York, N.Y. 10027*

Abstract

We study the effect of strong longitudinal color fields (SCF) in $p+p$ reactions up to Large Hadron Collider energies in the framework of the HIJING/B$\bar{\text{B}}$ v2.0 model that combines (collinear factorized) pQCD multiple minijet production with soft longitudinal string excitation and hadronization. The default vacuum string tension, $\kappa_0 = 1$ GeV/fm, is replaced by an effective energy dependent string tension, $\kappa(s) = \kappa_0(s/s_0)^{0.06}$ that increases monotonically with center-of-mass energy. The exponent $\lambda = 0.06$ is found sufficient to reproduce well the energy dependence of multiparticle observables in RHIC, Tevatron, as well as recent LHC data. This exponent is half of that predicted by the Color Glass Saturation (CGC) model, $\lambda_{CGC} = 0.115$, where gluon fusion multiparticle production mechanisms are assumed. In HIJING/B$\bar{\text{B}}$ v2.0, the rapid growth of $dN_{ch}/d\eta$ with energy is due to the interplay of copious minijet production with increasing of strong color field (SCF) contributions. The large (strange)baryon-to-meson ratios measured at Tevatron energies are well described. A significant enhancement of these ratios is predicted up to the highest LHC energy (14 TeV). The effect of J$\bar{\text{J}}$ loops and SCF on baryon-anti-baryon asymmetry, and its relation to baryon number transport, is also discussed.

PACS numbers: 12.38.Mh, 24.85.+p, 25.40Ve, 25.75.-q

I. INTRODUCTION

With the commissioning of the Large Hadron Collider (LHC), it will soon be possible to test models of multiparticle production in hadron-hadron collisions up to an energy of 14 TeV. Charged particle densities, $dN_{\rm ch}/d\eta$, especially the values at mid-rapidity and their dependence on center-of-mass energy $\sqrt{s}$ (c.m.s.) are important for understanding the mechanism of hadron production and the interplay of soft and hard scattering contributions in the LHC energy range. The rate of parton-parton and multi parton-parton (MPI) scattering are strongly correlated to the observed particle multiplicity (related also to *initial entropy* and *initial energy density* generated in the collision process). New data on inclusive charged particle distributions from the LHC in pp collisions have become available [1–12]. These results complement previous data on pp and $p\bar{p}$ collisions taken at lower energies $\sqrt{s} = 0.02$ - 1.96 TeV [13–23]. Many of these measurements have been used to constrain phenomenological models of soft-hadronic interactions and to predict properties at higher energies [25–38]. The recent LHC data may lead to a better theoretical understanding based on a Quantum Chromodynamics (QCD) approach [39–42].

The Heavy Ion Jet Interacting Generator (HIJING) [43] and HIJING/B$\bar{\rm B}$ v1.10 models [44] have been used extensively to study particle production in pp collisions and to determine the physical properties of the ultra-dense matter produced in relativistic heavy-ion collisions. In the LUND [45] and Dual-Parton (DPM) [46] models multi QCD strings or flux tubes were proposed to describe soft multiparticle production in longitudinal color fields. Color exchange between high x partons in the projectile and target create confined color flux tubes of tension ($\approx$ 1 GeV/fm), that must neutralize through pair production or color singlet hadronization approximately uniformly in rapidity. In nucleus-nucleus collisions, the $A^{1/3}$ enhancement of the local parton density of high x partons allows for higher color Casimir representations to be excited. Those flux tubes with stronger longitudinal color fields than in average pp reactions have been called color ropes [47] and naturally have higher string tensions [48]. Recently, an extension of Color Glass Condensate (CGC) theory has proposed a more detailed dynamical "GLASMA" model [49, 50] of color ropes.

In the HIJING model [43] the soft beam jet fragmentation is modeled by simple diquark-quark strings as in the LUND model with multiple gluon kinks induced by soft gluon radiations. Hard collisions are included with standard perturbative QCD (pQCD) as programmed

in the PYTHIA generator [51]. However, HIJING differs from PYTHIA by the incusion of a geometric scaling multiple jet production model. Thus this model contains both longitudinal field induced *soft* beam jet multiparticle production and collinear factorized pQCD based *hard* multiple jet production for $p_T \geq p_0 = 2$ GeV/c.

A systematic comparison with data on pp and $p\bar{p}$ collisions in a wide energy range [43] revealed that minijet production and fragmentation as implemented in the HIJING model provide a simultaneous and consistent explanation of several effects: the inclusive spectra at moderate transverse momentum (p_T); the energy dependence of the central rapidity density; the two particle correlation function; and the degree of violation of Koba-Nielsen-Olesen (KNO) scaling [52], [53] up to Tevatron energy ($\sqrt{s} = 1.8$ TeV). However, the model failed to describe the dependence of the mean value of transverse momentum ($< p_T >$) on charged particle multiplicity ($N_{\rm ch}$). Wang argued [53] that by requiring high $N_{\rm ch}$ within a limited pseudorapidity (η) range one necessarily biases the data towards higher p_T minijets, hence the observed increase of $< p_T >$ versus (vs.) $dN_{\rm ch}/d\eta$ [53]. This effect has also been associated with the presence of transverse flow of the hadronic matter [54, 55] and was proposed as possibly due to *quark-gluon plasma* (QGP) formation already in pp collisions.

Initial states of color gauge fields produced in high-energy heavy-ion collisions have also recently been discussed in Ref. [56]. Decay of a strong color electric field (SCF) ($E > E_{critical}$=10^{18} V/m) due to the Schwinger mechanisms [57] plays an important role at the initial stage of heavy-ion collisions at ultra-relativistic energies. A thermalization scenario based on the analogy between Schwinger mechanisms and the Hawking-Unruh effect has been proposed [58]. It was also suggested that the back-reaction and screening effects of quark and anti-quark pairs on external electric field could even lead to the phenomenon of plasma oscillations [59–61].

Recently, the Schwinger mechanism has been revisited [62] and pair production in time-dependent electric fields has been studied [63]. It was concluded that particles with large momentum were likely to have been created earlier, and for very short temporal widths ($\Delta\tau \approx 10{\rm t_c}$, where the Compton time ${\rm t_c} = 1/{\rm m_c}$) and as a consequence the Schwinger formula could underestimate the reachable particle number density. In previous papers, we have shown that the dynamics of strangeness production in pp and Au + Au collisions at Relativistic Heavy Ion Collider (RHIC) energies deviates considerably from calculations based on Schwinger-like estimates for homogeneous and constant color fields and point to

the contribution of fluctuations of transient strong color fields (SCF) [64–67].

In this paper we extend our study of the dynamic consequences of SCF in the framework of the HIJING/B$\bar{\text{B}}$ v2.0 model [65] to particle production in hadron-hadron collisions at LHC energies. We explore dynamical effects associated with long range coherent fields (*i.e*, strong longitudinal color fields, SCF), including baryon junctions and loops [64, 68], with emphasis on the new observables measured in *pp* collisions at the LHC by the ALICE, ATLAS and CMS collaborations. Our study aims to investigate a broad set of observables sensitive to the dynamics of the collisions, covering both longitudinal and transverse degree of freedom. In addition, this study is intended to provide the *pp* baseline to future extrapolations to LHC studies of proton-nucleus ($p + A$) and nucleus-nucleus ($A + A$) collisions.

II. OUTLINE OF HIJING/B$\bar{\text{B}}$ V2.0 MODEL.

In HIJING/B$\bar{\text{B}}$ v2.0, in addition to conventional quark-diquark longitudinal electric fields, novel color flux topology junction anti-junction (J$\bar{\text{J}}$) loops are also implemented. In a dual superconductor model of color confinement for the three-quark positioning in a Y - geometry, the flux tubes converge first toward the center of the triangle and there is also another component that runs in the opposite direction (like a *Mercedes star*) [69]. Unlike the conventional diquark-quark implemented in LUND and the HIJING model [43], the HIJING/B$\bar{\text{B}}$ v1.10 [44] model allows the diquark-quark to split with the three independent flux lines tied together with an ϵ_{ijk} a junction and terminating on three delocalized fundamental Casimir quarks. We introduced [68] a new version (v2.0) of HIJING/B$\bar{\text{B}}$ that differs from HIJING/B$\bar{\text{B}}$ v1.10 [44] in its implementation of additional more complex flux topologies via junction anti-junction (J$\bar{\text{J}}$) loops. We parametrize the probability that a junction loop occurs in the string. Moreover, we enhance the intrinsic (anti)diquark-quark p_T kick (by a factor $f = 3$) of all (q-qq) strings that contain one or multiple J$\bar{\text{J}}$ loops. The reason for this is the mechanism behind the dynamic of diquark-quark breaking (see Ref. [65] for details).

In string fragmentation phenomenology, it has been proposed that the observed strong enhancement of strange particle production in nuclear collisions could be naturally explained via strong color field (SCF) effects [48] . For a uniform chromoelectric flux tube with field (E), the pair production rate [47, 48, 62] per unit volume for a (light)heavy quark (Q) is

given by

$$\Gamma = \frac{\kappa^2}{4\pi^3}\exp\left(-\frac{\pi\, m_Q^2}{\kappa}\right), \tag{1}$$

where Q = qq (diquark), s (strange), c (charm) or b (bottom). The *current quark masses* are $m_{\rm qq} = 0.45$ GeV [70], $m_s = 0.12$ GeV, $m_{\rm c} = 1.27$ GeV, and $m_b = 4.16$ GeV [71]. The *constituent quark masses* of light non-strange quarks are $M_{u,d} = 0.23$ GeV, of the strange quark is M_s=0.35 GeV [72], and of the diquark is $M_{\rm qq} = 0.55 \pm 0.05$ GeV [70].

Note that $\kappa = |eE|_{eff} = \sqrt{C_2(A)/C_2(F)}\,\kappa_0$ is the effective string tension in low energy pp reactions with $\kappa_0 \approx 1$ GeV/fm and $C_2(A)$, $C_2(F)$ are the second order Casimir operators (see Ref. [48]). An enhanced rate for spontaneous pair production is naturally associated with "*strong chromo-electric fields*", such that $\kappa/m_{\rm Q}^2 > 1$ *at least some of the time*. In a strong longitudinal color electric field, the heavier flavor suppression factor $\gamma_{Q\bar{Q}}$ varies with string tension via the well known Schwinger formula [57], since

$$\gamma_{Q\bar{Q}} = \frac{\Gamma_{Q\bar{Q}}}{\Gamma_{q\bar{q}}} = \exp\left(-\frac{\pi(M_Q^2 - m_q^2)}{\kappa_0}\right) < 1 \tag{2}$$

for Q = qq, s, c or b and $q = u$, d. In our calculations, we assume that $M_{qq}^{\rm eff} = 0.5$ GeV, $M_s^{\rm eff} = 0.28$ GeV, $M_c^{\rm eff} = 1.30$ GeV. Therefore, the above formula implies a suppression of heavier quark production according to $u : d :$ qq $: s : c \approx 1 : 1 : 0.02 : 0.3 : 10^{-11}$ for the vacuum string tension $\kappa_0 = 1$ GeV/fm. For a color rope, on the other hand, if the *average string tension* value κ increases, the suppression factors $\gamma_{Q\bar{Q}}$ increase. We show below that this dynamical mechanism improves considerably the description of the strange meson/hyperon data at the Tevatron and at LHC energies.

Saturation physics is based on the observation that small-x hadronic and nuclear wave functions, and, thus the scattering cross sections as well, are described by the same internal momentum scale known as the *saturation scale* ($Q_{\rm sat}$). A recent analysis of pp data up to LHC 7 TeV has shown that, with the k_T factorized (GLR) gluon fusion approximation [73], the growth of the $dN_{ch}/d\eta$ can be accounted for if the saturation scale grows with c.m.s. energy as

$$Q_{\rm sat}^2(s) = Q_0^2(s/s_0)^{\lambda_{\rm CGC}}, \tag{3}$$

with $\lambda_{\rm CGC} \approx 0.115$. The saturation scale is also increasing with atomic number as $A^{1/6}$ [58]. It was argued that the effective string tension (κ) of color ropes should scale with $Q_{\rm sat}^2$ [58, 59].

However, in HIJING the string/rope fragmentation is the only soft source of multiparticle production and multiple minijets provide a semi-hard additional source that is computable within collinear factorized standard pQCD with initial and final radiation (DGLAP evolution [74]). In order to achieve a quantitative description, within our HIJING/B$\bar{\text{B}}$ framework we will show that combined effects of hard and soft sources of multiparticle production can reproduce the available data in the range $0.02 < \sqrt{s} < 20$ TeV only with a reduced dependence of the effective string tension on $\sqrt{s}$. We find that the data can be well reproduced taking

$$\kappa(s) = \kappa_0 \ (s/s_0)^{0.06} \ \text{GeV/fm} \approx Q_0 \, Q_{\text{sat}}(s), \tag{4}$$

where $\kappa_0 = 1$ GeV/fm is the vacuum string tension value, $s_0 = 1$ GeV^2 is a scale factor, and Q_0 is adjusted to give $\kappa = 1.88$ GeV/fm at the RHIC energy $\sqrt{s} = 0.2$ TeV. Our phenomenological $\kappa(s)$ is compared to $Q^2_{\text{sat}}(s)$ in Fig. 1, where $\kappa = 1.40$ GeV/fm at $\sqrt{s} = 0.017$ TeV increases to $\kappa = 3.14$ GeV/fm at $\sqrt{s} = 14$ TeV.

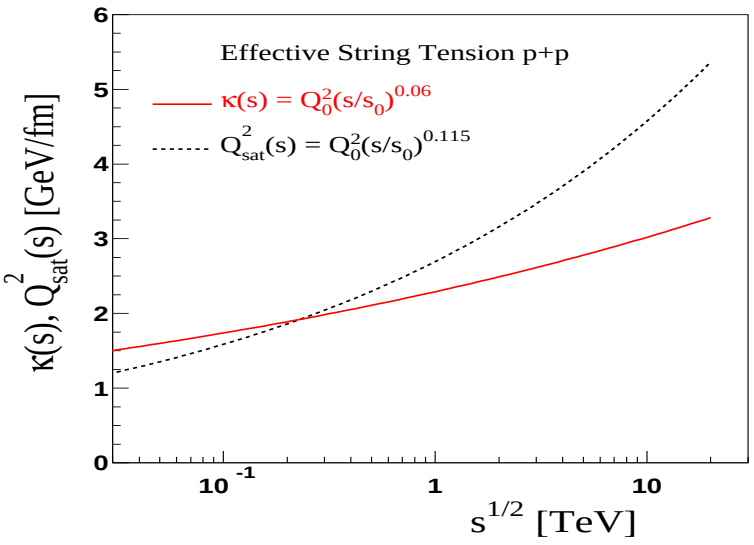

FIG. 1: (Color online) Energy dependence of the effective string tension $\kappa(s)$ in pp collisions (Eq. 4). The values Q^2_{sat} (Eq. 3) are from CGC model fits to LHC data from Ref. [30].

The energy dependence of the string tension leads to a variation of the diquark/quark suppression factors, as well as the enhanced intrinsic transverse momentum k_T. These include i) the ratio of production rates of diquark-quark to quark pairs (diquark-quark suppression factor), $\gamma_{\text{qq}} = P(\text{qq}\overline{\text{qq}})/P(q\bar{q})$; ii) the ratio of production rates of strange to non-strange quark pairs (strangeness suppression factor), $\gamma_s = P(s\bar{s})/P(q\bar{q})$; iii) the extra

suppression associated with a diquark containing a strange quark compared to the normal suppression of strange quark (γ_s), $\gamma_{us} = (P(\mathrm{us}\overline{\mathrm{us}})/P(\mathrm{ud}\overline{\mathrm{ud}}))/(\gamma_s)$; iv) the suppression of spin 1 diquarks relative to spin 0 ones (apart from the factor of 3 enhancement of the former based on counting the number of spin states), γ_{10}; and v) the (anti)quark ($\sigma''_q = \sqrt{\kappa/\kappa_0}\cdot\sigma_q$) and (anti)diquark ($\sigma''_{\mathrm{qq}} = \sqrt{\kappa/\kappa_0}\cdot f\cdot\sigma_{\mathrm{qq}}$) Gaussian width. As an example we plot in Fig. 2 the energy dependence of the suppression factor $\gamma_s = s/u$, when the string tension values $\kappa(s)$ are taken from Eq. 4 in comparison with the values predicted using Q^2_{sat} (Eq. 3 from the CGC model fit [30]).

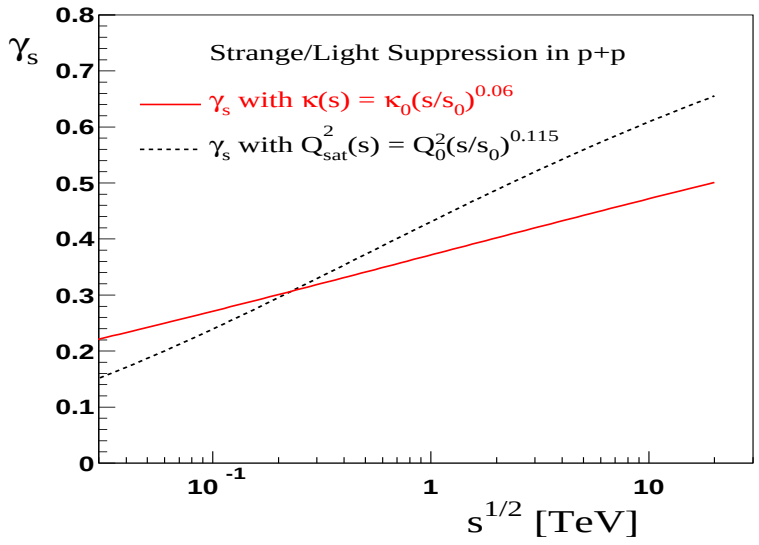

FIG. 2: (Color online) Energy dependence of the strange to light quark suppression factors, $\gamma_s = s/u$, using $\kappa(s)$ from Eq. 4 and using $Q^2_{\mathrm{sat}}(s)$ from Ref. [30] are compared. (Note that this Schwinger suppression factor is not used in the CGC model).

The contributions of multiple jets to the multiplicity distributions in pp and $p\bar{p}$ collisions have been studied in detail in Ref. [75]. Within the HIJING model, one assumes that nucleon-nucleon collisions at high energy can be divided into soft and hard processes with at least one pair of jet production with $p_T > p_0$. A cut-off scale p_0 in the transverse momentum of the final jet production has to be introduced below which the interaction is considered non-perturbative and can be characterized by a finite soft parton cross section σ_{soft}. The inclusive jet cross section σ_{jet} at leading order (LO) [76] is

$$\sigma_{jet} = \int_{p_0^2}^{s/4} \mathrm{d}p_T^2 \mathrm{d}y_1 \mathrm{d}y_2 \frac{1}{2} \frac{\mathrm{d}\sigma_{jet}}{\mathrm{d}p_T^2 \mathrm{d}y_1 \mathrm{d}y_2}, \tag{5}$$

where,

$$\frac{\mathrm{d}\sigma_{jet}}{\mathrm{d}p_T^2\mathrm{d}y_1\mathrm{d}y_2} = K\sum_{a,b} x_1 f_a(x_1,p_T^2) x_2 f_b(x_2,p_T^2)\frac{\mathrm{d}\sigma^{ab}(\hat{s},\hat{t},\hat{u})}{\mathrm{d}\hat{t}} \tag{6}$$

depends on the parton-parton cross section σ^{ab} and parton distribution functions (PDF) $f_a(x,p_T^2)$. The summation runs over all parton species; y_1 and y_2 are the rapidities of the scattered partons; x_1 and x_2 are the light-cone momentum fractions carried by the initial partons. The factor $K \approx 2$ accounts for the next-to-leading order (NLO) corrections to the leading order jet cross section. In the default HIJING model (v.1.383), the Duke-Owens parameterization [77] of PDFs in nucleons is used. With the Duke-Owens parameterization of PDFs, an energy independent cut-off scale p_0 =2 GeV/c and a constant soft parton cross section $\sigma_{soft} = 57$ mb are sufficient to reproduce the experimental data on total and inelastic cross sections and the hadron central rapidity density in $p+p(\bar{p})$ collisions [52, 53]. Our results have been obtained using the same set of parameters for hard scatterings as in the latest version of HIJING (v1.383).

III. CHARGED PARTICLES

A. Charged Hadron Pseudorapidity

Charged hadron multiplicity measurements are the first results of the LHC physics program. Data for *pp* collisions were reported by the ALICE, ATLAS, and CMS collaborations [1–11]. The new data at mid-rapidity for non single diffractive interactions (NSD) and inelastic scattering (INEL) are shown in Fig. 3, which includes also similar results at lower energies. The main result is an observed sizeable increase of the central pseudorapidity density with c.m.s. energy.

The main contribution to the multiplicity comes from soft interactions with only a small component originating from hard scattering of the partonic constituents of the proton. In contrast to the higher p_T regime, well described by pQCD, particle production in soft collisions is generally modeled phenomenologically to describe the different *pp* scattering processes: elastic scattering (el), single diffractive (SD), double diffractive dissociation (DD), and inelastic non-diffractive scattering (ND). Experimentally, minimum bias events are a close approximation of NSD interactions, *i.e.*, $\sigma_{\rm NSD} = \sigma_{\rm tot} - \sigma_{\rm el} - \sigma_{\rm SD}$, where $\sigma_{\rm tot}$ is the total cross section. The selection of NSD events is energy dependent and differs somewhat for dif-

ferent experimental triggers. The event selection of inelastic processes (INEL) includes SD interactions: $\sigma_{\rm INEL} = \sigma_{\rm tot} - \sigma_{\rm el}$. The data therefore must be corrected for the SD component, involving model dependent calculations.

The results of the model calculations for both NSD (left panel) and INEL (right panel) are also shown in Fig. 3. Solid lines depict results including the strong color field (SCF) effects whereas the results without SCF effects are shown as dashed lines. Without SCF effects the model strongly overestimates the central charged particle density. The absolute value and energy increase of the central rapidity density are well reproduced assuming the energy dependent string tension given in Eq. 4. At higher LHC energies (2.36 and 7 TeV), a discrepancy of 10-15 % is observed.

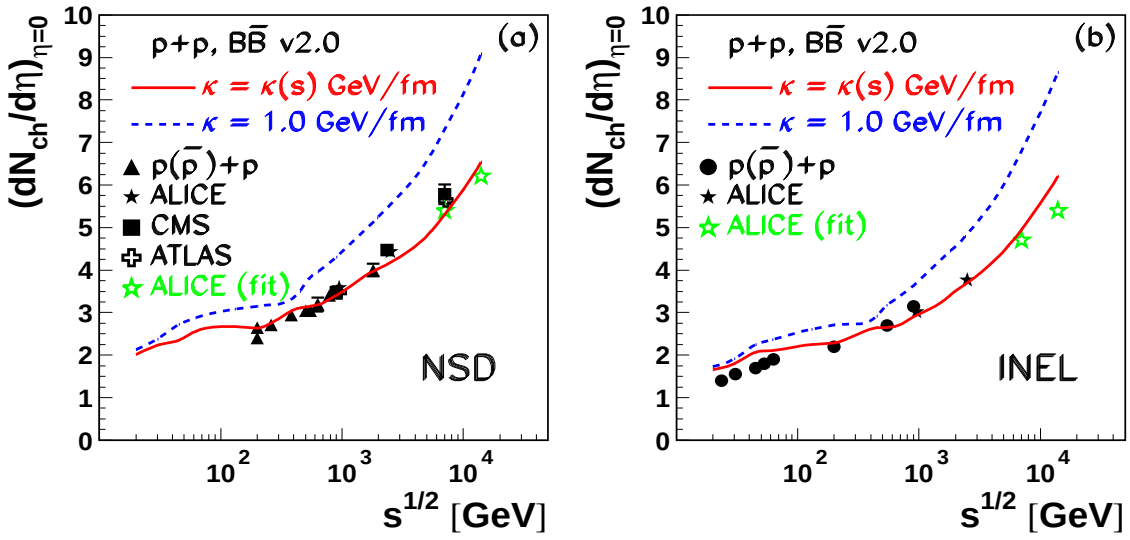

FIG. 3: (Color online) Comparison of HIJING/B$\bar{\rm B}$ v2.0 predictions for central charged particle pseudorapidity density in pp and $p\bar{p}$ interactions for non-single-diffractive (NSD) (left panel) and inelastic (INEL) (right panel) interactions as a function of c.m.s. energy. The solid and dashed lines are the results with and without SCF, respectively. The data are from Refs. [1–3, 6, 10, 16–19, 21] (left panel) and from Refs. [3, 19, 21, 23] (right panel). Only statistical error bars are shown. The open stars at 7 and 14 TeV (ALICE fit), are obtained by a power law fit to lower energy data from Refs. [6], [35].

As the colliding energy increases, the rate of multiple parton interactions (MPI) also increases, producing a rise in the central multiplicity. The increase with energy in our phenomenology is due to the interplay of the increased mini-jet production in high colliding

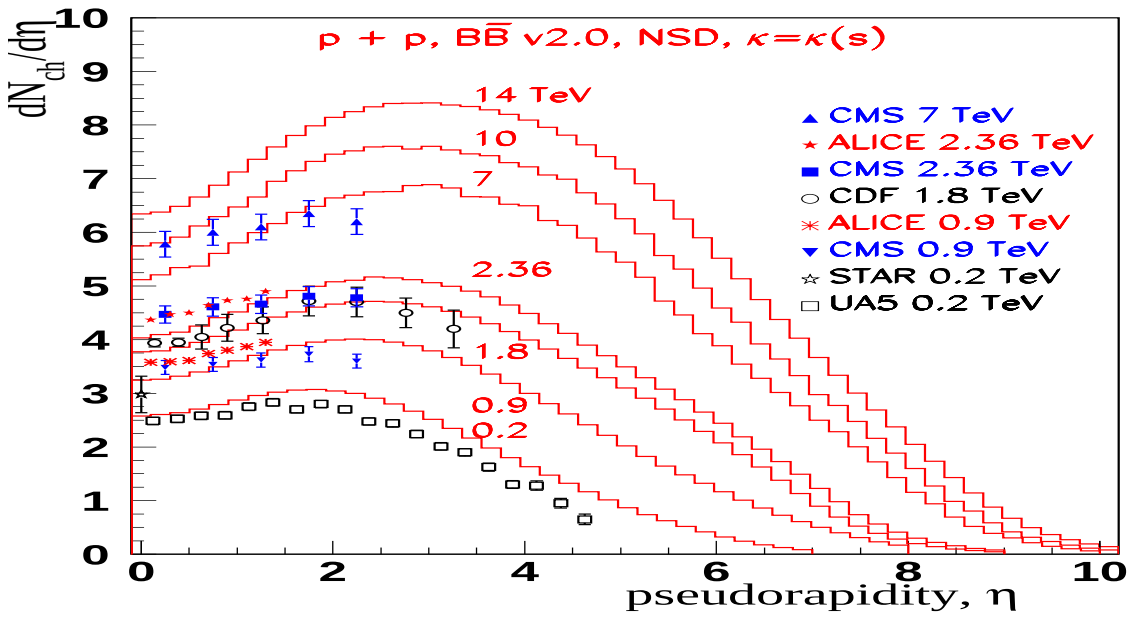

FIG. 4: (Color online) Comparison of HIJING/BB̄ v2.0 predictions for the pseudorapidity distribution of charged particles in $p + p$ ($\bar{p}$) collisions at various c.m.s. energies. The solid histograms are the results with SCF and JJ̄ loops. The data are from Refs. [22] (UA5), [13] (STAR), [17] (CDF), [3, 5] (ALICE), [1, 2] (CMS). Only statistical error bars are shown.

energy with SCF effects. For an increase of strangeness suppression factors due to an increase of string tension with energy ($\kappa = \kappa(s)$), the model predicts a decrease of produced pions due to energy conservation. Lower values of $\kappa(s)$ imply smaller values for strangeness suppression factors, therefore a higher multiplicity of mesons (mostly pions).

Changing the effective value $\kappa(s) = 2.89$ GeV/fm to $\kappa(s) = 2.0$ GeV/fm results in an increased multiplicity of 11% at 7 TeV where the effect is greatest. In addition, the multiplicity depends also on the value of the cut-off parameter p_0. Low values of p_0 imply high rates of parton-parton scattering and hence high levels of particle multiplicity. Evidently for increasing values of p_0 the opposite is expected. At 7 TeV, where the effect is also the largest, changing p_0 by $\pm\,0.5$ GeV results in a change of only $\mp\,1.8\%$ for the central pseudorapidity density.

Data on the charged particle pseudorapidity distribution are also available over a limited η range [1, 2] [3, 5, 6]. These are presented in Fig. 4 where we also include results obtained at 0.2 TeV by the UA5 [22] and STAR [13] collaborations, and with CDF results [17] obtained

at the Tevatron for $p\bar{p}$ collisions at 1.8 TeV. Consistent with the discussion above, a scenario with SCF effects (solid histograms) reproduces the measured multiplicity distributions well. At all energies considered, theoretical calculations predict a central dip at mid-rapidity that is consistent with the observations. At 0.9 and 2.36 TeV, the shape of the distribution measured by the ALICE collaboration is very well reproduced, while the CMS results show a much flatter distributions than calculated (also the case at 7 TeV). Data over a larger rapidity range are needed to determine the shape of the falling density in the fragmentation region. For completeness, predictions at 10 and 14 TeV, the higher LHC energies, are also shown.

B. Transverse momentum spectra

The measured transverse momentum distributions for NSD events over an energy range $\sqrt{s} = 0.63 - 7$ TeV are shown in Fig. 5. These recent measurements are performed in the central rapidity region and cover a wide p_T range ($0.15 < p_T < 10$ GeV/c), where both hard and soft processes are expected to contribute. The data of ATLAS and CMS are measured in larger pseudorapidity intervals ($|\eta| < 2.5$). In contrast, ALICE and CDF measurements are in a very central region ($|\eta| < 0.8$ and $|\eta| < 1.0$, respectively). The calculation takes into account the difference in acceptance, but as can be concluded from Fig. 4, this difference in pseudorapidity range has a negligible effect on the measured cross section.

The model calculations including SCF effects describe the data well at $\sqrt{s} = 0.63$ TeV, but lead to a harder spectrum that observed at higher energy. The model gives a fair description of the spectral shape at low p_T but overestimate the data at high p_T. The discrepancy is highest (up to a factor of three) at $\sqrt{s} = 7$ TeV. We do not understand the source of this discrepancy and await higher p_T data to draw a firm conclusion. However, in our phenomenology this could indicate that jet quenching, *i.e.* suppression of high p_T particles like that observed at RHIC energies in nucleus-nucleus collisions, could also appear in pp collisions in events with large multiplicity. This overestimation of high p_T yield leads also to a similar overestimation of the mean transverse momentum ($< p_T >$) and of the correlation of mean $< p_T >$ as a function of N_{ch}, which we do not discuss here.

Within our model we generate events with different numbers of mini-jets up to some maximum values. High numbers of mini-jets lead to higher multiplicity events. For events

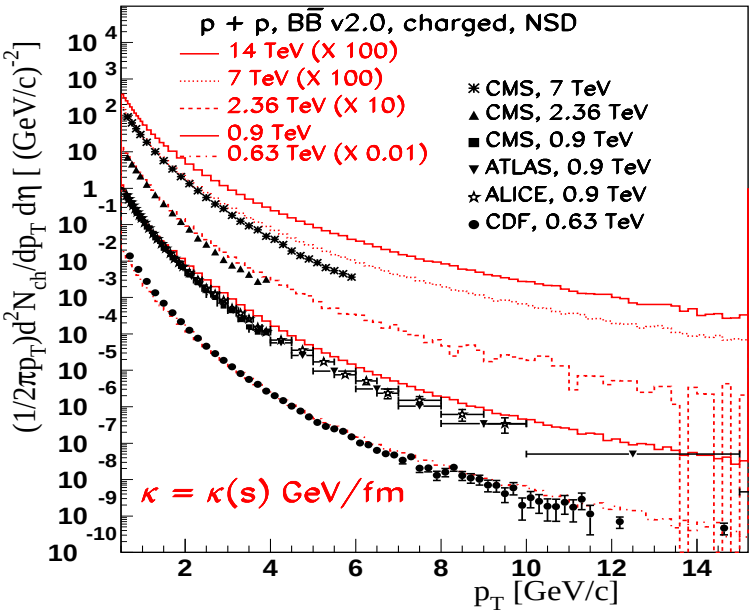

FIG. 5: (Color online) Comparison with data of HIJING/B$\bar{\text{B}}$ v2.0 predictions of charged-hadron transverse momentum distributions at LHC energies. The calculated spectra include the combined effects of SCF and J$\bar{\text{J}}$ loops. The histograms and data have been scaled for clarity by the factors indicated. The data are from Refs. [24] (CDF), [4] (ALICE), [7] (ATLAS), [1, 2] (CMS). Error bars include only the statistical uncertainties.

with ten mini-jets (the maximum assumed in our calculation), the central charged particle pseudorapidity density could increase up to ≈ 20 and the total multiplicity could be greater than 150 at Tevatron energy (1.8 TeV). The measurements of two particle correlations over the entire azimuth could reveal the jet structure related to high p_T particles [78]. The study of these correlations in events with high multiplicity could help us to draw a firm conclusion with regard to a possible jet quenching phenomenon in pp collisions.

IV. IDENTIFIED PARTICLE SPECTRA AND RATIOS

A. Baryon-to-Meson ratio

The pp single particle inclusive p_T spectra measurements are important for understanding collision dynamics, since the various particles show different systematic behavior, as observed at RHIC energy [78]. Detailed theoretical predictions for single inclusive hadron production

(including strange hyperons) are discussed in this section. Baryon-to-meson ratios (B/M) are experimental observables that can be used at the LHC for investigating multi-parton interactions and helping to understand the underlying physics [79–81].

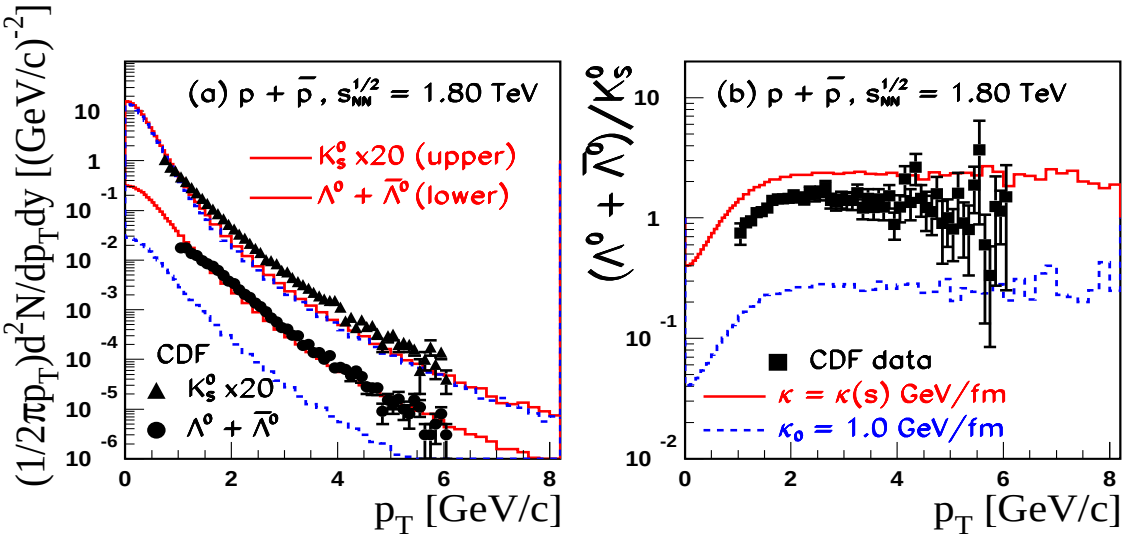

FIG. 6: (Color online) HIJING/BB̄ v2.0 predictions at $\sqrt{s}$ = 1.8 TeV of baryon and mesons transverse momentum at mid-rapidity ($-1 < y < 1$) (a) and their ratios for single strange particles $(\Lambda^0+\bar{\Lambda}^0)/K^0_S$ (b) in minimum bias $p\bar{p}$ collisions. The solid and dashed lines have the same meaning as in Fig. 3. Experimental results at $\sqrt{s} = 1.8$ TeV are from Ref. [86] (CDF Collaboration). Error bars include only the statistical uncertainties. The ratios (b) have been calculated by us, dividing the spectra in the panel (a).

Unexpectedly high B/M ratios observed in $A + A$ collisions have been discussed in terms of recombination and coalescence mechanisms [82–84]. Such high ratios at intermediate p_T were also reported in pp collisions at RHIC [85] and at the Tevatron [86]. In pp collisions, however, a coalescence/hadronization scenario is not favored due to low phase space density in the final state. Our HIJING/BB̄ model, with SCF effects included, provides an alternative dynamical explanation of the heavy-ion data at RHIC energies. We have shown that the model also predicts an increasing yield of (multi)strange particles, thereby better describing the experimental data [65].

Figure 6 (b) shows a comparison of model predictions with CDF experimental data [86] of the strange baryon-to-meson ratio $(\Lambda^0 + \bar{\Lambda}^0)/K^0_S$ at 1.8 TeV. The particle p_T spectra are shown in the panel (a). The measured ratio is fairly well described within our phenomenol-

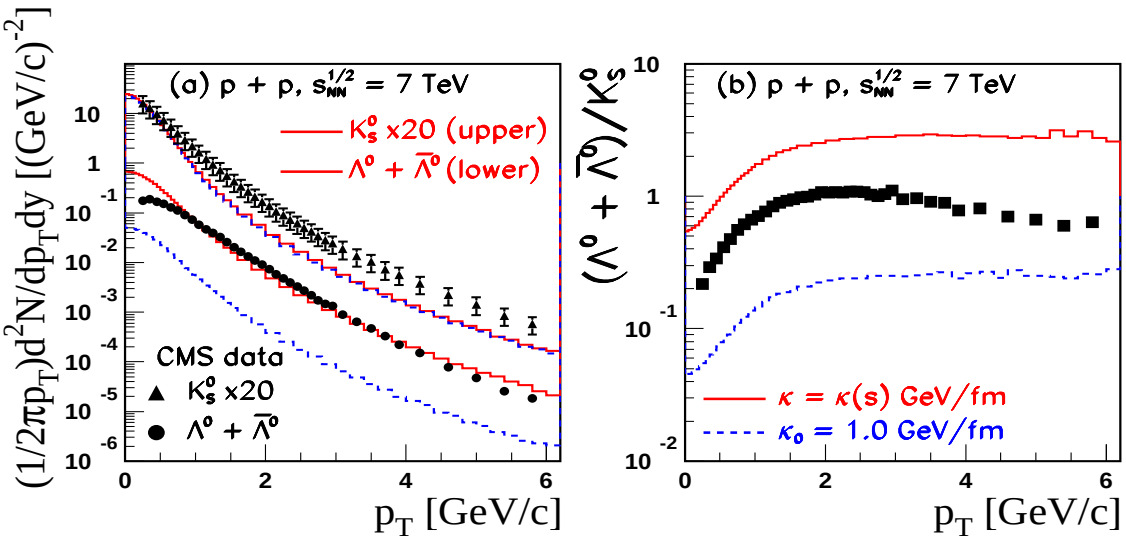

FIG. 7: (Color online) Predictions of the HIJING/B$\bar{\text{B}}$ v2.0 model for baryon and mesons transverse momentum in the rapidity range $-2 < y < 2$ (a) and their ratio (b) for minimum bias $p\bar{p}$ collisions at $\sqrt{s} = 7.0$ TeV. The solid and dashed lines have the same meaning as in Fig. 3. The experimental results (a) are from Ref. [87](CMS Collaboration) . Error bars include only the statistical uncertainties. The ratios (b) have been calculated by us, dividing the spectra in the panel (a).

ogy. The larger string tension parameterization results in a predicted increase of the ratio $(\Lambda^0 + \bar{\Lambda}^0)/K_S^0$ by a factor of ≈ 10 at the Tevatron energy. The p_T spectra show that the increased ratio is due almost entirely to an increase of the Λ cross section that is well described with $\kappa(s) = \kappa_0\ (s/s_0)^{0.06}$ GeV/fm. The model underestimates the kaon production by 15-25 %.

The model predictions at 7 TeV, currently the maximum energy where there are data [87], are shown in Fig. 7 (b). The model gives a good description of hyperon production $(\Lambda^0 + \bar{\Lambda}^0)$, for which an increase by a factor of ten is still predicted if SCF effects are considered. However, our calculations underestimate by approximately a factor of two the yield of K_S^0 and, as a consequence, result in a higher ratio than that observed. This result needs further investigation (theoretical and experimental) on heavy flavour production at this energy. We note that the models PYTHIA [88, 89] and Energy-conserving Partons Off-shell remnants and Spliting of partons ladders (EPOS) [90, 91] cannot reproduce the observed high B/M ratio (see Fig. 6 and Fig. 7 from Ref. [80]). The preliminary data reported by the CMS collaboration indicate high hyperon yield. Comparisons with PYTHIA results show that

this model significantly underestimates the hyperon yields in pp collisions at 0.9 and 7 TeV [87].

The strange particle ratios could also be the manifestation of new collective phenomena. In the EPOS model such an increase is obtained if the production of a *mini-plasma* is considered in pp collisions [25], [91]. If confirmed by future measurements, the study of these observables could open a perspective on new physics in pp interactions.

Similar conclusions are obtained from the study of the proton/pion (p/π^+, $\bar{p}/\pi^-$) ratios where data exist at lower energies [92, 93]. These data, shown in Figure 8, are limited to low $p_T < 2$ GeV/c. Adding SCF effects results in a very sizable increase of the ratio and our calculations provide a good description of the data in the measured range. However, as the calculations indicate, to draw a final conclusion measurements at intermediate and high p_T are needed.

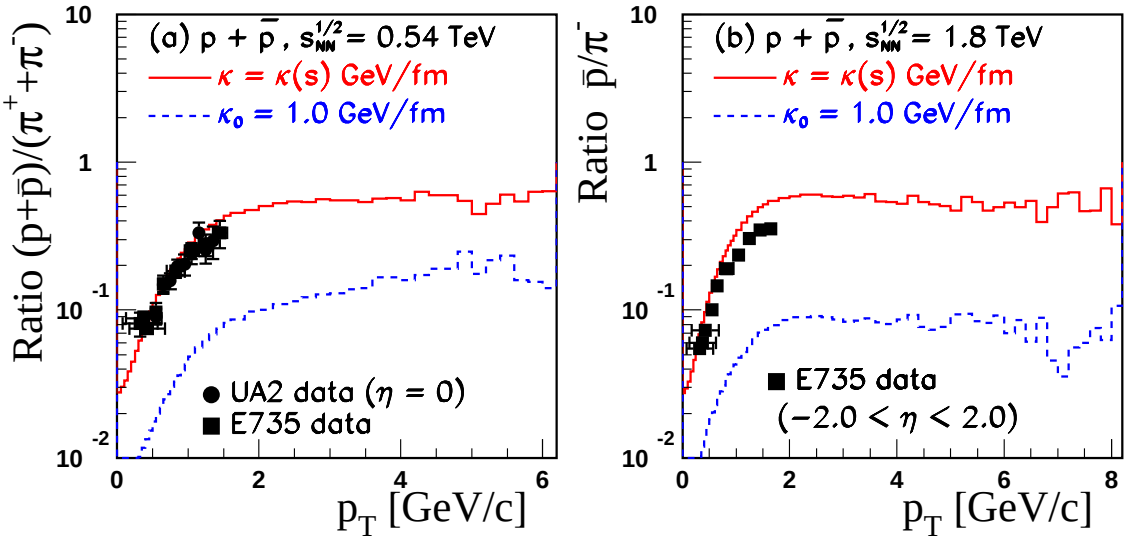

FIG. 8: (Color online) Comparison of HIJING/B$\bar{\text{B}}$ v2.0 predictions with data on the non-strange baryon over meson ratios from minimum bias events in the rapidity range $|y| < 2$. The solid and dashed lines have the same meaning as in Fig. 3. Experimental results for $|y| < 2$ at $\sqrt{s} = 0.54$ TeV (left panel) and at $\sqrt{s} = 1.8$ TeV (right panel) are from Ref. [92] (E735 Collaboration). The results at mid-rapidity at $\sqrt{s} = 0.54$ TeV (left panel) are from Ref. [93] (UA2 Collaboration). Error bars include only the statistical uncertainties.

To the extent that the LHC experiments are able to identify hadron species, such data will provide vital input to validate this interpretation. The model predictions at LHC energies

for the p_T dependence of the $\bar{p}/\pi^-$ ratio are shown in Fig. 9. An enhancement up to the highest LHC energy and a weak energy dependence, with a saturation that sets in for a c.m.s. energy $\sqrt{s} > 2.36$ TeV, is predicted. Note that preliminary data at 0.9 TeV reported by the ALICE collaboration for p_T spectra of pions (π^+) and protons (p) [94] cover to $p_T < 2.5$ GeV/c. The model results, with SCF effects included (dot-dashed histogram in Fig. 9) are consistent with a p/π^+ ratio derived from the spectra reported by ALICE at 0.9 TeV in Ref. [94].

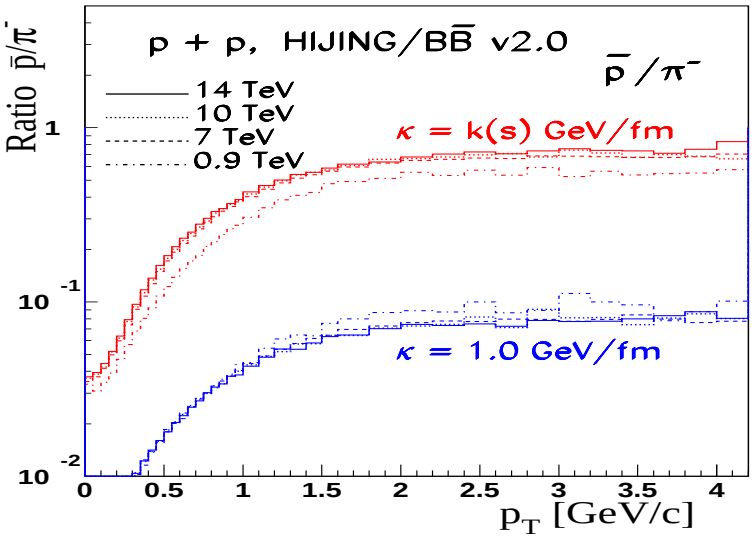

FIG. 9: (Color online) Predictions of the HIJING/B$\bar{\text{B}}$ v2.0 model of non-strange baryon over meson ratios ($\bar{p}/\pi^-$) for minimum bias events at mid-rapidity at LHC energies. The upper curves correspond to calculations which include the effects of SCF and J$\bar{\text{J}}$ loops. The lower curves corresponds to calculations without SCF effects. The results are at 0.9 TeV (dot dashed-histograms), at 7 TeV (dashed histograms), at 10 TeV (dotted histograms) and at 14 TeV (solid histograms).

In our approach, the dynamical mechanism that leads to such high values of B/M ratios is SCF appearing at the initial stage of the interaction. The SCF mechanism strongly modifies the fragmentation processes (strangeness suppression factors) and thus results in a huge increase of (strange)baryons. This interpretation is also supported by more sophisticated theoretical calculations, in a scenario in which a time-dependent pulse for the initial strength of the color field is considered [95, 96]. The large enhancement of the baryon-to-meson ratios demonstrates that SCF could play an important role in multiparticle production in pp collisions at LHC energies and that high energy density fluctuations can reach very high

densities, potentially comparable to those reached in central Au + Au collisions at RHIC energies [97].

B. Baryon-anti-baryon asymmetry

From the study of the baryon-anti-baryon asymmetry one can learn about the mechanism of baryon number transport. Baryon production via the conventional default quark-diquark mechanisms in the Lund string model are known to be inadequate even in $e^+ + e^-$ phenomenology. This is one of the main reasons for our continued exploration of alternative baryon junction mechanisms. The details of the new implementation of J$\bar{\text{J}}$ loops in HIJING/B$\bar{\text{B}}$ v2.0 are described in Ref. [65] Sec II A. In HIJING/B$\bar{\text{B}}$ v2.0 the main two mechanisms for baryon production are quark-diquark ($q-$qq) string fragmentation and junction anti-junction (J$\bar{\text{J}}$) loops [69] in which baryons are produced approximately in pairs. In a junction loop a color flux line splits at some intermediate point into two flux lines at one junction and then the flux lines fuse back at an anti-junction somewhere further along the original flux line. The distance in rapidity between these points is chosen via a Regge distribution [65]. We assume that, out of the non single diffractive nucleon-nucleon (NN) interaction cross section ($\sigma_{\rm NSD}$), a fraction $f_{J\bar{J}} = \sigma_{J\bar{J}}/(\sigma_{\rm INEL} - \sigma_{\rm SD})$ of the events excite a junction loop. The probability that the incident baryon has a J$\bar{\text{J}}$ loop in p(A)+A collisions after $n_{\rm hits}$ simulated binary collisions is given by

$$P_{J\bar{J}} = 1 - (1 - f_{J\bar{J}})^{n_{hits}}, \tag{7}$$

where $\sigma_{J\bar{J}} = 17$ mb, $\sigma_{\rm SD}$ is parametrized in the model, and the total inelastic nucleon-nucleon cross sections are calculated [43]. These cross sections imply that a junction loop occurs in *pp* collisions with a rather high probability (at RHIC energy $f_{J\bar{J}} \approx 0.5$ for $\sigma_{\rm INEL} =$ 42 mb). Taking a constant value for $\sigma_{J\bar{J}}$ results in a decrease with energy of the probability $P_{J\bar{J}}$, due to a faster increase with energy of $\sigma_{\rm INEL}$ relative to $\sigma_{\rm SD}$. The actual probability is modified also by string fragmentation processes for which we consider a threshold cutoff mass $M_c = 6$ GeV/c^2 in order to have enough kinematic phase space to produce B$\bar{\text{B}}$ pairs. We have investigated the sensitivity of the results to the value of parameters $\sigma_{J\bar{J}}$ and M_c and found no significant variation on pseudorapidity distributions of charged particles for 15 mb $< \sigma_{J\bar{J}} <$ 25 mb and for 4 GeV/c^2 $< M_c <$ 6 GeV/c^2.

Baryon number transport is quantified in terms of the rapidity loss ($\delta y_{\rm loss} = \delta y_{\rm beam} - \delta y_{\rm baryon}$, where $y_{\rm beam}$ and $y_{\rm baryon}$ are the rapidity of incoming beam and outgoing baryon, respectively) and has been discussed within our model phenomenology for $A + A$ collisions in Refs. [64–66]. It was shown that HIJING/B$\bar{\rm B}$ v1.0 overestimate the stopping power and give a mild energy dependence of net-baryons at mid-rapidity. The energy dependence of net-baryons at mid-rapidity per participant pair within HIJING/B$\bar{\rm B}$ v2.0 is proportional to $(s/s_0)^{-1/4+\Delta/2}$, similar to the dependence predicted in Ref. [98], with the assumption that J$\bar{\rm J}$ is the dominant mechanism. This dependence is obtained assuming the following parameters [66]: $s_0 = 1$ GeV^2 (the usual parameter of Regge theory), $\alpha(0) = 1/2$ (the reggeon intercept of the trajectory), and $\alpha_P(0) = 1 + \Delta$ (where $\Delta \approx 0.01$) for the pomeron intercept.

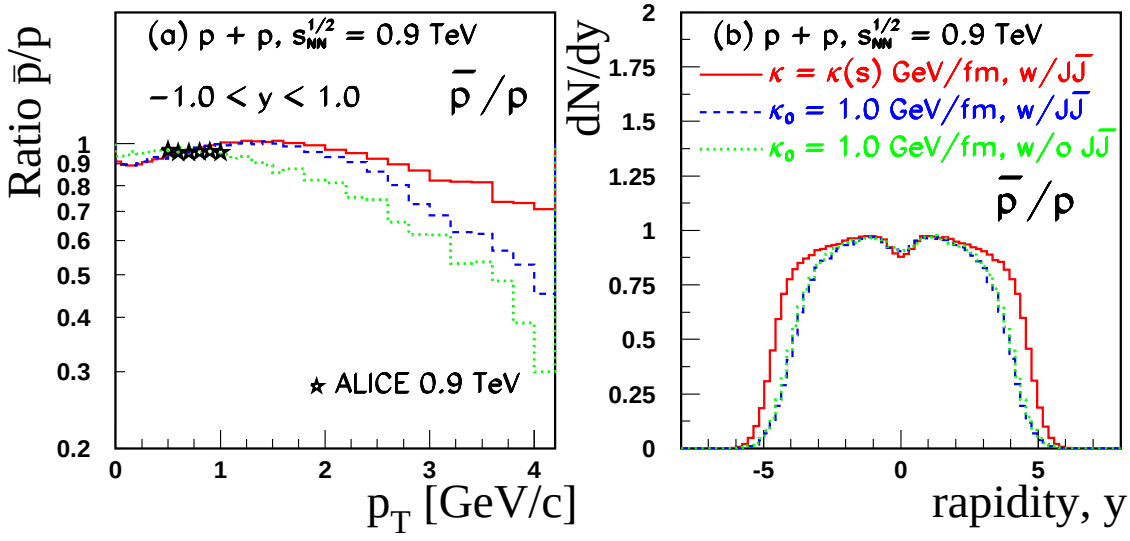

FIG. 10: (Color online) HIJING/B$\bar{\rm B}$ v2.0 predictions p_T distributions (a) at mid-rapidity for the $\bar{p}/p$ ratio at $\sqrt{s} = 0.9$ TeV; rapidity distributions are shown in part (b). The results are from three possible scenarios: without contributions from SCF and J$\bar{\rm J}$ loops (dotted histograms), including only the effect of J$\bar{\rm J}$ loops (dashed histograms) and including both effects (SCF and J$\bar{\rm J}$ loops) (solid histograms). The data are from Ref. [99] (ALICE Collaboration). Only statistical errors are shown.

Recently, the ALICE Collaboration reported results [99] on mid-rapidity anti-proton-to-proton ratio in pp collisions at $\sqrt{s} = 0.9$ and 7 TeV and equivalently the proton-anti-proton asymmetry, $A = (N_p - N_{\bar{p}})/(N_p + N_{\bar{p}})$. These data could be used to constrain Regge inspired model descriptions of baryon asymmetry. The authors state that, within statistical

errors, the observed $\bar{p}/p$ ratio shows no dependence on transverse momentum or rapidity in the limited measured acceptance ($-0.8 < y < 0.8$; $0 < p_T < 1$ GeV/c). In Fig. 10 (a) are compared the HIJING/B$\bar{\text{B}}$ v2.0 model predictions with the published data at 0.9 TeV. Our model predicts negligible dependence on p_T for $0 < p_T < 2$ GeV/c, and a slight p_T dependence at higher p_T, where both effects (J$\bar{\text{J}}$ loops and SCF) could contribute. The full calculation is shown by the solid histogram. The dotted line is the prediction without J$\bar{\text{J}}$ loops and SCF effects while the dashed line includes the effect of J$\bar{\text{J}}$ loops only. Over the measured ranges the rapidity distribution of the ratio $\bar{p}/p$ distribution is not sensitive to the various scenarios presented. The scenario with combined effects results in a wider rapidity distribution at $y > 3$ (b). The narrow structure observed near $y = 0$ has no physical significance and we believe that it is likely due to a numerical artifact of our current implementation of fragmentation scheme.

Separate proton and anti-proton rapidity distributions are, however, much more sensitive to SCF effects, as seen in Fig. 11. The model predicts a substantial increase (by a factor of ≈ 5) for p($\bar{p}$), when SCF are taken into account. Due to the high cutoff mass $M_c = 6$ GeV/c^2 the effect of J$\bar{\text{J}}$ loops is very small over the entire rapidity region. Analysis of the 7 TeV data leads to similar conclusions, but shows less effect at high p_T.

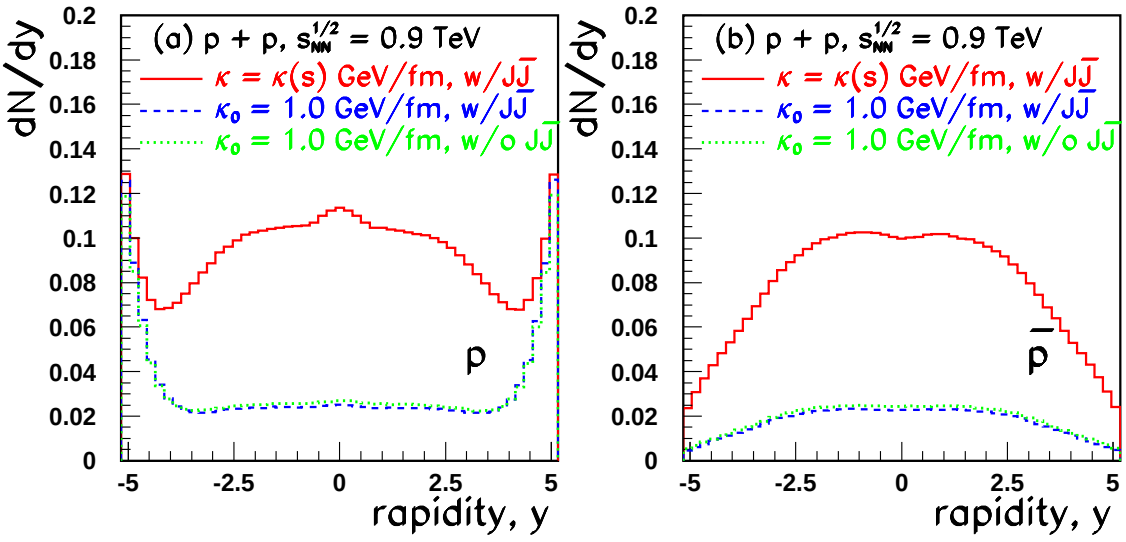

FIG. 11: (Color online) Predictions of the HIJING/B$\bar{\text{B}}$ v2.0 model for rapidity distributions of protons (a) and anti-protons (b) at $\sqrt{s} = 0.9$ TeV. The histograms have the same meaning as in Fig. 10.

Over the measured range the feed-down-corrected data for the $\bar{p}/p$ ratio rises from 0.957 ± 0.006 at 0.9 TeV to 0.991 ± 0.005 at 7 TeV [99]. Although the measured mid-rapidity ratio is close to unity there is a small but significant excess of protons over anti-protons corresponding to an asymmetry of $A = 0.022 \pm 0.003$ and $A = 0.005 \pm 0.003$ at $\sqrt{s} = 0.9$ and 7 TeV, respectively. Within our model using a Regge intercept of $\alpha_0 = 1/2$ results in a proton-anti-proton asymmetry $A_{\rm model} = 0.032$ (0.002) at 0.9 TeV (7 TeV). The result overestimates the value of asymmetry at 0.9 TeV. These values show that a fraction of the baryon number associated with the beam particles is transported over rapidity intervals of less than seven units. However, a better understanding of the baryon transport would require measuring the rapidity dependence of the asymmetry over a larger range.

In Ref. [65] we discuss the predicted rapidity correlation length for production of baryon-anti-baryon pairs within our model. The predicted rapidity correlation length $(1 - \alpha(0))^{-1}$ depends upon the value of the Regge intercept $\alpha(0)$ [44]. A value of $\alpha(0) \simeq 0.5$ leads to rapidity correlations in the range $|y_B - y_{\bar{B}}| \sim 2$, while a value $\alpha(0) \simeq 1.0$ [100] is associated with infinite range rapidity correlations. This kind of analysis and future measurements at LHC energies will help us to determine better the specific parameters characterizing $\mathrm{J\bar{J}}$ loops used in the calculations of baryon number transport and/or baryon-anti-baryon asymmetry while helping to establish the validity of Regge inspired models.

V. SUMMARY AND CONCLUSIONS

We have studied the influence of strong longitudinal color fields and of possible multi-gluon dynamics (*gluon junctions*) in particle production in pp collisions, with a focus on RHIC, to Tevatron, and LHC energies. We have investigated a set of observables sensitive to the dynamics of the collisions, covering both longitudinal and transverse degree of freedom. A detailed comparison with newly available experimental data from the LHC has been performed.

We found that the inclusion of the multiple minijet source limits the growth of the string tension $\kappa(s)$ to be approximately only linear as a function of saturation scale $Q_{\rm sat}$ (Eq. 4), in contrast to recent approaches [30] where $\kappa(s)$ scales as $Q^2_{\rm sat}$ (Eq. 3). The reason for this is that in the CGC model the collinear factorized minijet mechanism is suppressed by geometric scaling to much higher p_T. Future measurements at LHC energies ($\sqrt{s} = 7$ and

14 TeV), extended to high p_T, will help to clarify the validity of this mechanism.

We have shown that SCF could play an important role in particle production at mid-rapidity in pp collisions. Our calculations show that high-energy density fluctuations in pp collisions at LHC can reach densities comparable to those reached in central nuclear $(A+A)$ collisions at RHIC. A large enhancement of the (strange)baryon-to-meson ratios that persists up to the highest LHC energy can be explained as an effect of SCF that appears at the initial stage of the interaction. The mechanisms of hadron production are very sensitive to the early phase of the collisions, when fluctuations of the color field strength are highest. Strong Color Field effects are modeled by varying the effective string tension that controls the $q\bar{q}$ and $\mathrm{qq}\overline{\mathrm{qq}}$ pair creation rates and strangeness suppression factors. SCF, therefore, may modify the fragmentation processes with a resultant huge increase of (strange)baryons.

We show that both $\mathrm{J}\bar{\mathrm{J}}$ loops and SCF effects could play an important role in baryon (anti-baryon) production at mid-rapidity in pp collisions at LHC energies. Introducing a new $\mathrm{J}\bar{\mathrm{J}}$ loop algorithm in the framework of HIJING/$\mathrm{B}\bar{\mathrm{B}}$ v2.0 leads to a consistent and significant improvement in the description of the recent experimental results for proton-anti-proton and for baryon-anti-baryon asymmetry in comparison to the older versions HIJING/B or HIJING/$\mathrm{B}\bar{\mathrm{B}}$ v1.0 [44]. We have shown that baryon number transport is suppressed for $\delta y > 7$, a result that is confirmed by recent ALICE measurements [99].

The present study is limited to the effect of initial state baryon production via possible junction dynamics in strong fields. It would be very useful to consider a generalization of back reaction effects [59] to the case not only of pair production relevant for mesons but to the more difficult three string junction configurations needed to describe baryon production.

A greater sensitivity to SCF effects is expected also for open charm and bottom production [67]. In particular, measurements of rapidity and p_T distributions for particles involving charm and bottom quark, would provide an important test of the relevance of SCF fluctuations, helping us to determine values of the suppression factors $\gamma_{Q\bar{Q}}$ (where Q = qq, s, c, b), which have strong dependence on the main parameters of QCD (the constituent and current quark masses) and on the system size. Even though the success of this procedure has been clearly illustrated here, a fuller understanding of particle production and especially of (multi)strange particles in ultra-relativistic pp collisions at the LHC remains an exciting open question, and will continue to challenge many theoretical ideas.

VI. ACKNOWLEDGMENTS

Acknowledgments: We thank S. Das Gupta and S. Jeon for useful discussions and continued support. We thank P. Levai for helpful discussions and suggestions throughout this project. VTP acknowledges computer facilities at Columbia University, New York, where part of these calculations were performed. This work was supported by the Natural Sciences and Engineering Research Council of Canada. This work was also supported by the Division of Nuclear Science, of the U. S. Department of Energy under Contract No. DE-AC03-76SF00098 and DE-FG02-93ER-40764.

---

[1] V. Khachatryan *et al.* [CMS Collaboration], JHEP **1002**, 041 (2010).

[2] V. Khachatryan *et al.* [CMS Collaboration], Phys. Rev. Lett. **105**, 022002 (2010).

[3] K. Aamodt *et al.* [ALICE Collaboration], Eur. Phys. J. C **65**, 111 (2010).

[4] K. Aamodt *et al.* [ALICE Collaboration], Phys. Lett. B **693**, 53 (2010).

[5] K. Aamodt *et al.* [ALICE Collaboration], Eur. Phys. J. C **68**, 345 (2010).

[6] K. Aamodt *et al.* [ALICE Collaboration], Eur. Phys. J. C **68**, 89 (2010).

[7] G. Aad *et al.* [ATLAS Collaboration], Phys. Lett. B **688**, 21 (2010).

[8] G. Aad *et al.*, ATLAS Collaboration, ATLAS-CONF-2010-024.

[9] G. Aad *et al.*, ATLAS Collaboration, ATLAS-CONF-2010-031.

[10] G. Aad *et al.*, ATLAS Collaboration, ATLAS-CONF-2010-046.

[11] G. Aad *et al.*, ATLAS Collaboration, ATLAS-CONF-2010-047.

[12] G. Aad *et al.*, ATLAS Collaboration, arXiv:1012.5104 [hep-ex] (submitted to New J. of Phys.).

[13] B. I. Abelev *et al.* [STAR Collaboration], Phys. Rev. C **79**, 034909 (2009).

[14] T. Aaltonen *et al.*, CDF Collaboration, Phys. Rev. D **79**, 112005 (2009).

[15] T. Alexopoulos *et al.*, E735 Collaboration, Phys. Lett. B **336**, 599 (1994).

[16] C. Albajar *et al.*, UA1 Collaboration, Nucl. Phys. B **335**, 261 (1990).

[17] F. Abe *et al.*, CDF Collaboration, Phys. Rev. D **41**, 2330 (1990).

[18] R. E. Ansorge *et al.*, UA5 Collaboration, Z. Phys. C **43**, 357 (1989).

[19] R. E. Ansorge *et al.*, UA5 Collaboration, Z. Phys. C **37**, 191 (1988).

[20] F. Abe *et al.*, CDF Collaboration, Phys. Rev. Lett. **61**, 1819 (1988).

[21] G. J. Alner *et al.* Phys. Rep. **154**, 247 (1987).

[22] R. E. Ansorge *et al.*, UA5 Collaboration, Z. Phys. C **33**, 175 (1986).

[23] W. Thome *et al.*, Nucl. Phys. B **129**, 365 (1977).

[24] D. Acosta *et al.*, CDF Collaboration, Phys. Rev. D **65**, 072005 (2002).

[25] N. Armesto *et al.*, J. Phys. G **35**, 054001 (2008).

[26] N. Armesto, arXiv:0903.1330[hep-ph].

[27] M. Mitrovski, T. Schuster, G. Graf, H. Petersen and M. Bleicher, Phys. Rev. C **79**, 044901 (2009).

[28] E. Levin and A. H. Rezaeian, Phys. Rev. D **82**, 014022 (2010).

[29] E. Levin and A. H. Rezaeian, Phys. Rev. D **82**, 054003 (2010).

[30] L. McLerran and M. Praszalowicz, Acta Phys. Polon. B **41**, 1917 (2010).

[31] C. Merino, C. Pajares, M. M. Ryzhinskiy, and Yu. M. Shabelski, arXiv:1007.3206[hep-ph].

[32] P. Z. Skands, Phys. Rev. D **82**, 074018 (2010).

[33] A. Buckley, H. Hoeth, H. Schulz and J. E. von Seggern, PoS A **CAT08**, 112 (2009).

[34] A. Moraes, C. Buttar and I. Dawson, Eur. Phys. J. C **50**, 435 (2007).

[35] J. F. Grosse-Oetringhaus and K. Reygers, J. Phys. G **37**, 083001 (2010).

[36] I. Kraus, J. Cleymans, H. Oeschler and K. Redlich, Phys. Rev. C **79**, 014901 (2009).

[37] A. B. Kaidalov and M. G. Poghosyan, Eur. Phys. J. C **67**, 397 (2010).

[38] E. K. G. Sarkisyan and A. S. Sakharov, Eur. Phys. J. C **70**, 533 (2010).

[39] A. Warburton [CDF and D0 Collaborations], PoS **HCP2009**, 013 (2009).

[40] M. H. Seymour, arXiv:1008.2927 [hep-ph].

[41] R. Sassot, P. Zurita and M. Stratmann, Phys. Rev. D **82**, 074011 (2010).

[42] W. T. Deng, X. N. Wang and R. Xu, arXiv:1008.1841 [hep-ph].

[43] X. N. Wang and M. Gyulassy, Comput. Phys. **83** (1994) 307; X. N. Wang, Phys. Rep. **280**, 287 (1997).

[44] S. E. Vance and M. Gyulassy, Phys. Rev. Lett. **83**, 1735 (1999).

[45] B. Andersson, G. Gustafson, B. Nilsson-Almqvist, Nucl. Phys. **B281**, 289 (1987).

[46] A. Capella, U. Sukhatme, C. -I. Tan *et al.*, Phys. Rept. **236**, 225-329 (1994).

[47] T. S. Biro, H. B. Nielsen and J. Knoll, Nucl. Phys. **B245**, 449 (1984).

[48] M. Gyulassy and A. Iwazaki, Phys. Lett. B. **165**, 157 (1985).

[49] F. Gelis, T. Lappi and L. McLerran, Nucl. Phys. **A828**, 149 (2009); T. Lappi and L. McLerran, Nucl. Phys. **A772**, 200 (2006).

[50] L. McLerran, J. Phys. G **35**, 104001 (2008).

[51] T. Sjostrand, Comput. Phys. Commun. **82**, 74-90 (1994).

[52] X. N. Wang and M. Gyulassy, Phys. Rev. D **44**, 3501 (1991).

[53] X. N. Wang and M. Gyulassy, Phys. Rev. D **45**, 844 (1992).

[54] P. Levai and B. Muller, Phys. Rev. Lett. **67**, 1519 (1991).

[55] T. Pierog, S. Porteboeuf, I. Karpenko and K. Werner, arXiv:1005.4526 [hep-ph].

[56] A. Iwazaki, arXiv:0904.1449 [hep-ph].

[57] J. S. Schwinger, Phys. Rev. **82**, 664 (1951).

[58] D. Kharzeev, E. Levin and K. Tuchin, Phys. Rev. C **75**, 044903 (2007).

[59] N. Tanji, Annals Phys. **324**, 1691 (2009).

[60] R. Ruffini, G. Vereshchagin and S. S. Xue, Phys. Rept. **487**, 1 (2010).

[61] N. Tanji, Annals Phys. **325**, 2018 (2010).

[62] T. D. Cohen and D. A. McGady, Phys. Rev. D **78**, 036008 (2008).

[63] F. Hebenstreit, R. Alkofer and H. Gies, Phys. Rev. D **78**, 061701 (2008).

[64] V. Topor Pop, M. Gyulassy, J. Barrette, C. Gale, Phys. Rev. C **72**, 054901 (2005).

[65] V. Topor Pop, M. Gyulassy, J. Barrette, C. Gale, S. Jeon and R. Bellwied, Phys. Rev. C **75**, 014904 (2007) (and references therein).

[66] N. Armesto *et al.*, J. Phys. G **35**, 054001 (2008); V. Topor Pop *et al.*, *ibidem*, pp 15-18; V. Topor Pop *et al.*, *ibidem*, pp 57-59.

[67] V. Topor Pop, J. Barrette and M. Gyulassy, Phys. Rev. Lett. **102**, 232302 (2009).

[68] V. Topor Pop, M. Gyulassy, J. Barrette, C. Gale, X. N. Wang, N. Xu, Phys. Rev. C **70**, 064906 (2004).

[69] G. Ripka, Lecture Notes in Physics, **639**, 2004 (Ed.Springer, Berlin, Germany).

[70] M. Cristoforetti, P. Faccioli, G. Ripka, and M. Traini, Phys. Rev. D **71**, 114010 (2005).

[71] K. Nakamura *et al.* [Particle Data Group], J. Phys. G **37**, 075021 (2010).

[72] N. S. Amelin, N. Armesto, C. Pajares, and D. Sousa, Eur. Phys. J. C **22**, 149 (2001).

[73] L. V. Gribov, E. M. Levin and M. G. Ryskin, Phys. Rept. **100**, 1 (1983).

[74] G. Altarelli and G. Parisi, Nucl. Phys. **B126**, 298 (1977).

[75] X. N. Wang, Phys. Rev. D **43**, 104 (1991).

[76] E. Eichten, I. Hinchliffe, K. D. Lane and C. Quigg, Rev. Mod. Phys. **56**, 579 (1984) [Addendum-ibid. **58**, 1065 (1986)].

[77] D. W. Duke and J. F. Owens, Phys. Rev. D **30**, 49 (1984).

[78] M. J. Tannenbaum, arXiv:1008.1536 [nucl-ex].

[79] B. Hippolyte, Eur. Phys. J. C **49**, 121 (2007).

[80] B. Hippolyte, Eur. Phys. J. C **62**, 237 (2009).

[81] H. Ricaud, A. Kalweit and A. Maire, J. Phys. G **37**, 094049 (2010).

[82] R. J. Fries, B. Muller, C. Nonaka and S. A. Bass, Phys. Rev. C **68**, 044902 (2003).

[83] V. Greco, C. M. Ko and P. Levai, Phys. Rev. C **68**, 034904 (2003).

[84] R. C. Hwa and C. B. Yang, Phys. Rev. C **67**, 034902 (2003).

[85] B. I. Abelev *et al.* [STAR Collaboration], Phys. Rev. C **75**, 064901 (2007).

[86] D. E. Acosta *et al.* [CDF Collaboration], Phys. Rev. D **72**, 052001 (2005).

[87] CMS Collaboration, CMS-PAS-QCD-10-007 (2010).

[88] T. Sjostrand, S. Mrenna and P. Z. Skands, Comput. Phys. Commun. **178**, 852 (2008).

[89] T. Sjostrand, S. Mrenna and P. Z. Skands, JHEP **0605**, 026 (2006).

[90] K. Werner, T. Hirano, I. Karpenko, T. Pierog, S. Porteboeuf, M. Bleicher and S. Haussler, Nucl. Phys. Proc. Suppl. **196**, 36 (2009).

[91] K. Werner, I. Karpenko and T. Pierog, J. Phys. Conf. Ser. **230**, 012026 (2010).

[92] T. Alexopoulos *et. al.*, E735 Collaboration, Phys. Rev. D **48**, 984 (1993).

[93] M. Banner *et. al.*, UA2 Collaboration, Phys. Lett. B **122**, 322 (1983).

[94] P. Antonioli, for the ALICE Collaboration, arXiv:1010.3735 [hep-ex].

[95] V. V. Skokov and P. Levai, Phys. Rev. D **78**, 054004 (2008).

[96] V. Skokov and P. Levai, PoS E **PS-HEP2009**, 456 (2009).

[97] A. Giovannini and R. Ugoccioni, Eur. Phys. J. C **36**, 309 (2004).

[98] D. Kharzeev, Phys. Lett. B **378**, 238 (1996).

[99] A. K. Aamodt *et al.* [ALICE Collaboration], Phys. Rev. Lett. **105**, 072002 (2010).

[100] B. Z. Kopeliovich and B. Povh, Phys. Lett. B **446**, 321 (1999).